Advances in Environmental Technology 3 (2022) 169-184

Iranian Reasearch Organization for Science and Technology (IROST)

Advances in Environmental Technology

Journal home page: https://aet.irost.ir/

Investigation of photocatalytic degradation of 2,4-dichlorophenol by heat treated Fe_3O_4/TiO_2/Ag loaded polycaprolactone/polyethylenglycole electrospun nanofibers

Amir Naghizadeh[1], Mohammad Ali Salehi[1*], Leila Mivehi[2]

[1] Department of Chemical Engineering, Faculty of Engineering, University of Guilan, Guilan, Rasht, Iran

[2] Department of Textile Engineering, Faculty of Engineering, University of Guilan, Guilan, Rasht, Iran

ARTICLE INFO

Document Type:
Research Paper

Article history:
Received 16 March 2022
Received in revised form
26 July 2022
Accepted 26 July 2022

Keywords:
Electrospinning
Nanofibers
Metallic nanocomposite
Catalyst loaded nanofiber

ABSTRACT

The electrospinning technique is utilized to physically load Fe_3O_4/TiO_2/Ag nanoparticles on PCL/PEG nanofibers scaffold for oxidative decomposition of 2,4-dichlorophenol as a model organic pollutant. The scaffold is used in order to eliminate the need for separation of the catalyst after treatment, thus, making the catalyst system recyclable and reusable. Prepared nanofibers were thermally processed to change the morphology to crystalline form to make them transparent to visible light which is a necessity for the function of photocatalysts. Different analysis techniques such as X-ray diffraction, transmission electron microscopy, UV/Vis spectrophotometry, and field emission electron microscopy were implemented to identify and characterize presented products. Kinetic performance of both particulate system and nanofiber system was determined. Prepared products demonstrated good catalytic activity by 53% decomposing the target pollutant in 180 minutes of visible light exposure. The new catalyst loaded nanofiber system maintained the decomposition performance of the particulate system and improved its reusability. Although this scaffold nanofiber based system demonstrates slightly lower pollutant removal performance in the first run compared to the ternary non-fixed particle system (53.12% vs 54.74%), it outperforms the non-fixed particulate system through 2nd and 3rd runs. The decomposition rate is improved from 52.37% to 52.81% in the 2nd run and from 48.08 to 51.02% for the 3rd run. This photocatalytic system can be used as a reusable efficient catalyst system for oxidative decomposing of 2,4-dichlorophenol.

1. Introduction

Utilizing oxidising agents to convert contaminants into less harmful chemicals is a process known as oxidative degradation. The method is used to clean up organically contaminated wastewater and other industrial effluents [1-3]. Different oxidative agents such as hydrogen peroxide, ozone, potassium permanganate, and more importantly metallic oxides in nano scale are a few of the oxidizing substances employed in this procedure. Many studies have successfully used this method

*Corresponding author: Tel: +989123598607
E-mail: salehi.guilan.che@gmail.com
DOI:10.22104/AET.2022.5546.1508

for removal of pollutants such as dyes, pesticides, and pharmaceutical wastes. [4-7]. Titanium dioxide (TiO_2) is a multipurpose substance that has potential uses in a variety of fields, including energy storage and photocatalysis. This metallic oxide is used as a photocatalyst in the degradation of organic pollutants. Upon exposure to ultraviolet light, reactive oxygen species such as $O_2^{\bullet-}$ (ROS) are produced by TiO_2, and for this reason, we observe its photocatalytic activity. The reactive oxygen species can then react with the pollutants and break them down into less harmful substances [8-10]. The large intrinsic band gap of TiO_2 is one of the major bottlenecks in developing artificial photosynthesis with TiO_2. The large band gap of 3.2 eV limits the photocatalytic activity of TiO_2 to ultraviolet light only. In other words, TiO_2 cannot absorb visible light which is the main source of energy from the sun. This limits its use in applications that require visible light absorption such as photocatalysis in its unprocessed form [11,12], Additionally, TiO_2 cannot retain its excited state after the absorption of ultraviolet light and the light introduced active electrons and holes recombine to inactivate its photocatalytic activity. This recombination rate is influenced by several factors such as the surface area of the catalyst, the crystal structure of TiO_2, and the presence of impurities [13,14]. TiO_2 is generally considered safe for use in consumer products and is widely used in sunscreens, cosmetics, and food products. However, there are concerns about the safety of TiO_2 nanoparticles which are used in some applications such as photocatalysis and photovoltaics. The toxicity of TiO_2 nanoparticles is still under investigation [15]. Doping TiO_2 with non-metals such as carbon and nitrogen is often reported as one of the most effective ways of increasing its photocatalytic activity under visible light. The doping process can be achieved by introducing impurities such as nitrogen, carbon, or metals into the TiO_2 lattice. Doping can also improve the photocatalytic activity of TiO_2 by reducing the recombination rate of electrons and holes [14,16,17]. Other ways to modify the band gap of TiO_2 include doping with metals such as silver, copper, and iron. Another way is to modify the crystal structure of TiO_2 by using different synthesis methods [13,18,19]. Metals like silver show plasmon resonance in the visible spectrum. For example, silver shows a strong surface plasmon resonance at wavelengths of 410–420 nm for nanoparticles. The surface plasmon resonance of silver nanoparticles can be tuned by changing the size and shape of the particles. Silver nanoparticles can be decorated over TiO_2 surface through the localized surface plasmon resonance (SPR) effect. The SPR effect of silver nanoparticles on TiO_2 surface can enhance light absorption and drive dye molecules to an excited state more effectively than far-field light [16]. Chlorophenols are a group of chemicals which are created when phenol is electrophilically halogenated with chlorine. There are 5 basic types and 19 different chlorophenols. Some chlorophenols are used as pesticides and herbicides. Others are used as antiseptics and disinfectants. [20-22]. 2,4-dichlorophenol is a dichlorophenol that is phenol carrying chloro substituents at positions 2 and 4. It is a colorless crystalline solid with a medicinal odor. Its melting point 45 °C and sinks in water which produces a mildly acidic solution. Strong irritant to tissues; toxic by ingestion. It is produced on a large scale as a precursor to the herbicide 2,4-dichlorophenoxyacetic acid (2,4-D). Additionally, it can be created as a byproduct of the production of various chlorinated chemicals, the chlorination of water and wood pulp, as well as the burning or incineration of municipal solid waste, coal, and wood [23-25]. It is also a photo-degradation product of the common antibacterial and antifungal agent triclosan along with the dioxin 2,8-dichlorodibenzo-p-dioxin. Breathing 2,4-Dichlorophenol can irritate the nose, throat and lungs causing coughing, wheezing and/or shortness of breath and may damage the liver and kidneys. Repeated exposure may affect the nervous system causing headache, dizziness, nausea, vomiting, weakness and even coma [26-28]. As a result, it will be critical to find new and effective solutions to reduce the environmental harm caused by chlorophenols. The other problem we are facing when using TiO_2 based particles is their separation after pollutant treatment of wastewater material [12,29]. Post treatment separation of TiO_2 based particles proved to be hard because it is very well dispersed in water. Traditional methods use techniques such as filtration or utilization of

external force fields such as centrifugation and magnetic field treatment [30,31]. Trenary microspheres of $Fe_3O_4/TiO_2/Ag$ is also studied as a recyclable catalyst system under UV and Visible light with great success (80% degradation after 100 min of light exposure) [32]. These methods usually result in the loss of catalysts and other resources. Here we investigate the possibility of loading particles on nanofibers by electrospinning technique. This process initially fixes the particles in polymer mesh with a large specific surface area to facilitate mass transfer. There are multiple studies concerning long term and in use stability of TiO_2 based nanocomposites [33-37]. It is reported that $Fe_3O_4/TiO_2/Ag$ system could be stored for 1 year when dried and in the dark [34]. In aqueous medium, the composite is stable for 3 weeks, and finally, when the medium is slightly acidic (0.1 M acetic acid solution) the catalyst system is stable for 1 week [34]. PCL is a biocompatible polymer that does not introduce a new form of pollution to the medium. This polymer, with a small addition of PEG, also is readily electrospinnable. This property makes it a viable candidate for producing nanoscale fibers with a large specific surface area. Additionally, PCL is one of the most chemically stable biocompatible polymers, the degradation of the molecular chain of PCL in neutral pH aqueous medium is reported to be around 6 months. Moreover, PCL can easily be converted to a crystalline phase (by heat treatment) to make it transparent to visible light. It is important because the metallic particles require light to perform their oxidative responsibility. Electrospun PCL nanofibers have been used as a scaffold by multiple researchers. In a study, the possibility of attaching Nickel nanoparticles on PCL/Chitosan electrospun nanofibers for degradation of nitrophenols. They were able to improve the activity and reusability of particles compared to simple Nickel nanoparticles [38]. In another study, palladium is loaded on electrospun Polyethyleneimine/PCL fibers. These fibers are used to oxidate 4-nitrophenol. PEI/PCL is here also used to physically stabilize Nickel nanoparticles and improve their usability [39]. On the contrary, PCL nanofibers are seldom used as a scaffold for photoactive catalysts because their opacity, presents a barrier for the light to reach the loaded catalyst particles. Thus, in this study, we employed thermal treatment to make the scaffold transparent to visible light. This novel alteration approach enables us to use the PCL based nanofiber system as a scaffold for holding metallic nanocatalysts for recycling purposes. Thus we used PCL, a biocompatible polymer, as a base for a scaffold that physically fixes nanocatalyst particles, and at the same time, makes them available for the decomposition process. A small amount of PEG is also added to the polymer mixture to make it electrospinnable. After the electrospinning process, the produced systems are opaque, thus they present a barrier against visible and UV light to reach the metallic particle loaded catalysts. For this reason, this catalyst loaded nanofibers are heat treated to make them transparent to visible light. Regarding the PCL based nanofibrous scaffold, it is reported that the fibers are structurally stable for 1 year in phosphate salinated buffer, but the molecular weight of PCL starts to decrease after 6 mounts [40]. In this study, we utilized the produced nanofibers to investigate their oxidative behavior on the decomposition of 2,4-dichlorophenol as a model organic pollutant. The results are compared to the catalyst in its powder particulate form. Figure 1 demonstrates the process of material preparation and processes used in this study. First, we introduce the materials and methods which are implemented in the study. These methods consist of procedures utilized to produce nanocatalysts and then how we loaded them on nanofibers. Thus, we have done an extensive identification of products. Finally, we investigated and compared the results, and presented the reader with our conclusions.

2. Materials and methods

2.1. Materials

Polycaprolactone (PCL) Pellets and Polyethylene glycol (PEG) with average molecular weights of respectively 80 and 10 kDa were purchased from Sigma Aldrich (Interlab A.S. Istanbul, Turkey). Fe_3O_4 nanoparticles were prepared from $Fe_3O_4{\cdot}7H_2O$ and $FeCl_3{\cdot}6H_2O$. Titanium isopropoxide, TIP, and $AgNO_3$ were obtained from Merk. High purity 2,4-dichlorophenol (98%) was purchased from Merk. Reagent grade solvents, including

acetone (99.5% purity), glacial acetic acid, ammonia, and ethanol were also purchased from Sigma Aldrich (Interlab A.S. Istanbul, Turkey).

2.2. Preparation of Fe_3O_4 nanoparticles

The co-precipitation approach was used to create Fe_2O_3 nanoparticles in this work. In distilled water, 0.7954 g of iron (II) chloride, $FeCl_2.4H_2O$, and 1.2974 g of iron (III) chloride, $FeCl_3$ were dissolved. Throughout the experiment, the mole ratio of iron (II) chloride to iron (III) chloride was held constant at 1:2. After that, the solution was stirred for 30 minutes on a hot plate using a magnetic stirrer. Different processing temperatures, pH, and stirring speeds were all controlled during the mixing processes. The combined solution was then separated by centrifugation at 4000 rpm for 15 minutes. The separated precipitate was dried in an oven at 100 °C for 24 hours. Finally, using a pestle and mortar, the dried dark brown precipitated sample was collected and crushed into powder form [41,42].

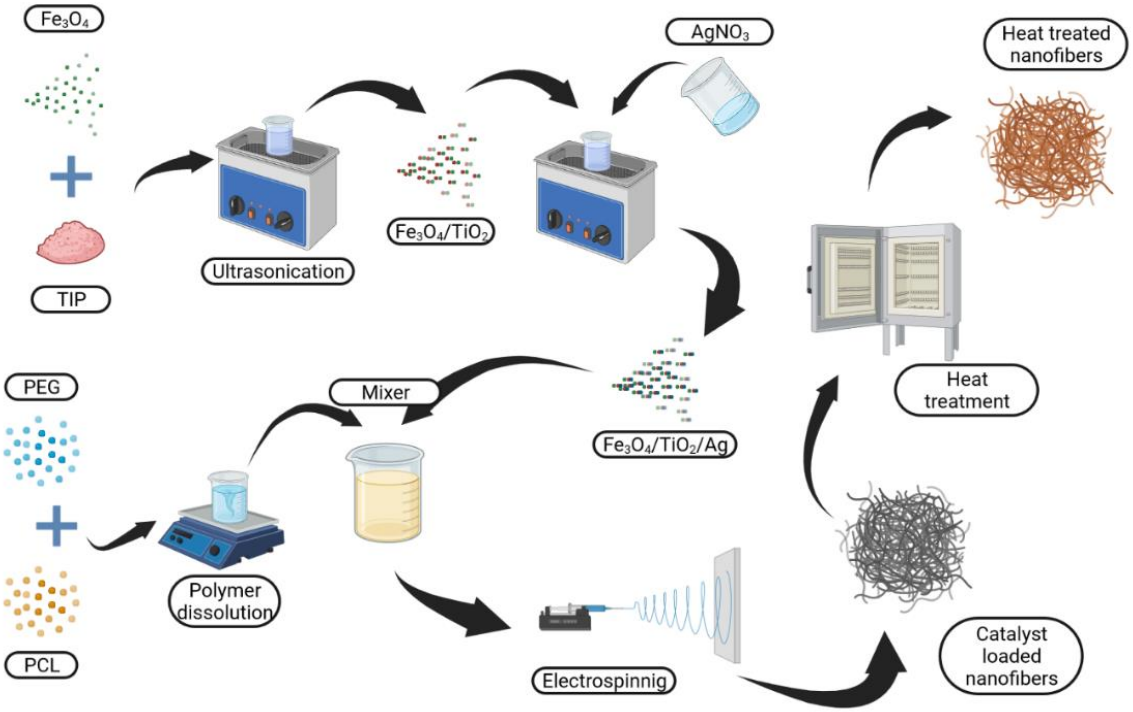

Fig. 1. Diagram of material preparation and processes.

2.3. Preparation of Fe_3O_4/TiO_2 nanostructure

The following steps were used to create the Fe_3O_4/TiO_2 composite. A solution of $FeCl_2.4H_2O$ (0.98 g) and $FeCl_3.6H_2O$ (2.4 g), with a mole ratio of 1:2, was vigorously agitated for 10 min before being purged with nitrogen to eliminate oxygen. A 25 weight percent NH_3H_2O solution was then used to bring the suspension's pH down to 10.0. After that, the suspension was transferred into a 100 mL flask and kept at 80 °C for 30 minutes in a water bath. Then, via magnetic attraction, the black precipitate was washed with 50% ethanol. The Fe_3O_4 NPs were then gradually added to a 4 mL 0.01 M TiF_4 solution and vigorously agitated for 10 min. After that, the suspension was put into a Teflon-sealed autoclave along with 50 mL of deionized water. For 48 hours, the autoclave was sealed and kept at 180 °C before being allowed to cool in room air. Magnetic separation was used to separate the reaction product from the final Fe_3O_4/TiO_2 Nanoparticles [43,44].

2.4. Preparation of $Fe_3O_4/TiO_2/Ag$ nanocomposite

TiO_2/Fe_3O_4 (0.50 g) was sonicated into suspension in deionized water (10 ml), to which $AgNO_3$ (0.46 ml, 100.0 mM) was gently added. After the mixture

had been stirred at 20 °C for 30 minutes, it had been homogenized, and Na_2CO_3 (0.5 ml, 1.0 percent w/v) had then been gradually added. The final slurry was filtered and allowed to air dry [6,45].

2.5. Preparation of PEG/PCL loaded solution

Solutions of PEG/PCL with a total concentration of 12.5%, (w/v) containing 1, 5, 10, 15, and 30% (w/w) of Fe_3O_4/TiO_2/Ag were prepared by dissolving an appropriate amount of PEG, PCL, and catalytic composted in a mixture solvent system of acetone/acetic acid (3/7 v/v), and then stirred for 6 hours to ensure complete dispersion.

2.6. Electrospinning of prepared solution

The electrospinning process was carried out using a custom-made electrospinning setup made by the authors of this manuscript at the chemical engineering faculty of the University of Guilan, which consists of a controllable relative humidity and temperature chamber, a high precision syringe pump, and a high voltage power supply. The prepared solutions were placed in air-sealed syringes attached to a 23G stainless steel needles with inner and outer diameters of respectively 0.33 mm and 0.64 mm. Subsequently, syringes were placed inside the electrospinning chamber. The high voltage power supply's positive electrode was connected to the needle, and the negative electrode was attached to the static circular stainless-steel disc collector. Before initiating any of the experiments, the temperature and relative humidity of the chamber were fixed at respectively 25±1 ℃ and 30±5 %. The flow rates of all processes were fixed at 0.5 mL/h. The nuzzle to collector distances of 10 cm with applied voltages of 26.5 kV resulted in electrical field intensities of 2.65 kV/cm [46]. The fiber formation process needed 4 hours to complete, to the extent that an appropriate amount of fiber would be available for further processing and evaluation steps.

2.7. Heat treatment of catalyst loaded nanofibers

The dried electrospun samples were thermally treated at 50 C for 5 hours in a vacuum oven. Through this process, PCL based nanofibers deform to crystalline morphology and appear transparent to visible light [47].

2.8. Identification and characterization

Field emission scanning electron microscopy (FESEM) was used to scan catalyst-loaded polymer systems (Tescan Mira3, Tescan Orsay Holding, a.s, Brno, Czech Republic). Hence, small pieces of polymer mats were cut out and placed on a metal slab and were gold-sputtered after a vacuum time of 20 minutes. Nanocomposite SEM images were produced by Vegall-Tescan SEM device equipped with elemental mapping. The absorbance spectra of samples were obtained using a Carry UV-50 UV-Vis spectrophotometer. Transmission electron microscopy (TEM Philips EM 208S) images of samples were obtained by collecting fibers on TEM mesh grids. For this purpose, mesh grids were installed on the collector disc of the electrospinning setup and the process was carried through for 1 minute to collect enough fibers for microscopy and prevent excessive fiber deposition. TEM made us able to determine the morphology and size of the core side of prepared samples. XRD analysis of prepared samples was carried out using an Xpert Pro Panalytical (Malvern Panalytical, Malvern, UK) X-ray diffractometer. The X-ray beam was produced using a 2.2 kW Cu-LFF anode at the voltage of 60 kV. The scan covered 2 theta angels in a range of 20-80 degree, at 1 /m rate.

2.9. Photocatalytic degradation of 2,4-dichlorophenol

In this study, 2,4-Dichlorophenol, a chlorinated derivative of phenol with the molecular formula $Cl_2C_6H_3OH$, is selected as a model organic pollutant. An OSRAM Halogen lamp was used as the light source in the degradation process. This light source produces light in a wavelength range of 350 to 800 nm and the emittance maximum is at 575 nm. Photocatalyst loaded nanofibers were cut in square shapes and were horizontally placed at the bottom of a beaker so that the surface area is normal to the light source. The beaker contains 100 mL of 40 ppm 2,4- dichlorophenol. Initially, the beaker is wrapped in an aluminum foil to block the ambient light. To ensure the chemical equilibrium on the fiber-solution interface, the fiber holding solution is mechanically stirred for 10 min before the photocatalytic oxidation process. Subsequently, the beaker is exposed to the light source for 180 min, and between certain time

intervals, 2 mL samples were gathered from the solution to spectrophotometrically analyze using a Carry UV-50 UV-Vis spectrophotometer.

3. Result and discussion

3.1. X-ray diffraction patterns and morphological studies

Figure 2 shows the XRD patterns of prepared Fe_3O_4, TiO_2/Fe_3O_4, $Fe_3O_4/TiO_2/Ag$, and nanofibers before and after heat treatment. Considering the Fe_3O_4 XRD pattern signifies characteristic diffractions at 2θ angles of 30.1°, 35.7°, 43.3°, 53.8°, 57.5° and 62.9°, which are consistent with the XRD pattern of Fe_3O_4 spinel reported in the literature [48]. This observation indicates that Fe_3O_4 nanoparticles are in their crystalline phase. Regarding the pure TiO_2 diffraction patterns, we can see peaks at 2θ = 25.4°, 37.6°, 48.0°, 53.8°, 55.1°, and 62.8°, which correspond to the crystalline state of TiO_2 in anatase phase [49]. Regarding the case of TiO_2/Fe_3O_4, we can see that the pattern predominantly matches the pattern of pure TiO_2, but at a lower intensity. Furthermore, some weak diffractions of Fe_3O_4 are also visible, suggesting that the Fe_3O_4 particles are coated with TiO_2 particles in the formation of the composite. If we look at diffraction patterns of $Fe_3O_4/TiO_2/Ag$, we can observe peaks at 2θ angles of 38.0°, 44.1°, 64.0°, and 77.3°. These peaks correspond to (111), (200), (220), and (311) planes of silver crystals which are consistent with the peaks reported in JCPDS database [50]. There is no diffraction peak of pure metallic silver present in the diffraction pattern of $Fe_3O_4/TiO_2/Ag$ due to its small size and low concentration in the composite matrix. Figure 2 also plots the X-ray diffraction of catalyst loaded nanofibers before and after heat treatment. The shape of plots predominantly resembles the XRD pattern of pure PCL because it is the main component of the system. This plot indicates that the fibers are initially in the amorphous phase, but after heat treatment, a sharp peak appears that suggests the shift to a crystalline state. Additionally, the peaks corresponding to that of $Fe_3O_4/TiO_2/Ag$ are small because of the low number of particles are present in the polymer matrix.

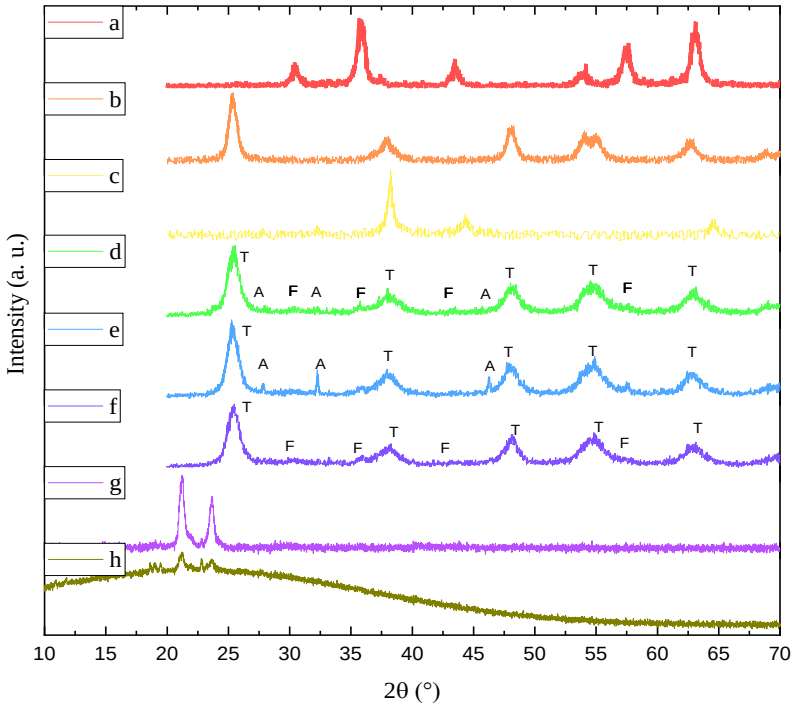

Fig. 2. XRD patterns of (a) Fe_3O_4, (b) TiO_2 (c) Ag (d) $Fe_3O_4/TiO_2/Ag$, (e) TiO_2/Ag, (f) TiO_2/Fe_3O_4 [45] and catalyst loaded fibers (h) before and (g) after heat treatment.

In order to find the average crystal size of the component we used the Scherrer equation as presented in equation 1:

$$D = k1 \cos q \quad (1)$$

Here, D, stands for average crystal size, l is the wavelength of X-ray beam (for Cu-LFF $\lambda = 1.54056Å$), b is the full with of diffraction at the half maximum radiation, K is a correction factor equals to 0.89, and q is peak angle diffraction. These parameters are displayed in Table 1. The anatase phase tetragonal lattice parameters of (101) crystal plane is calculated using equation (2).

$$1/d^2 = (k^2 + h^2)/a^2 + l^2/c^2 \quad (2)$$

Afterward, Braggs law was used to determine interplanar space, thus:

$$d_{hkl} = \frac{l}{2 \sin q} \quad (3)$$

The final step was to calculate the tetragonal cell volume. Eq. (4) is the geometrical relation to calculate cell volume:

$$V = a^2 c \quad (4)$$

Table 1. Crystal properties of the prepared samples [45].

Sample	Phase	Crystal Size (nm)	a,b (Å)	C (Å)	Cell Volume (Å^3)
TiO_2	anatase	10.35	3.75	9.60	136.30
TiO_2/Fe_3O_4	anatase	7.10	3.75	9.32	134.87
$Fe_3O_4/TiO_2/Ag$	anatase	8.15	3.75	9.00	127.75

Data presented in Table 1 suggests that lattice parameters are in good agreement with values presented in the literate. Since lattice parameters and XRD pattern of TiO_2 do not alter after the addition of other components, we can conclude that the addition of Fe_3O_4 and Ag onto TiO_2 preserves the TiO_2 anatase phase and additional components are deposited on the surface of TiO_2 rather than entering into a matrix structure.

3.2. Morphological study of prepared samples

Figure 3 shows the FESEM images of the produced $Fe_3O_4/TiO_2/Ag$ nanoparticles. This image demonstrates that Fe_3O_4 nanoparticles are wrapped by TiO_2 nanoparticles, and the nanocomposite is decorated by Ag at the top. This conclusion is derived from elemental mapping done over FESEM images of metallic oxide nanocomposites. These images indicate that Ti and Ag sit on the outer layer of the nanoparticles of Fe_3O_4. By examining these results, we can calculate the composition of each element in the system. Table 2 presents the numerical values for these parameters. Figure 4 shows the TEM images of metallic particles in which the gray TiO_2 surrounds the Fe_3O_4 particles represented in dark color. The bright Ag atoms particles are also scattered throughout the composite. Figure 5 demonstrates the FESEM images of the prepared electrospun nanofibers before and after the heat treatment. The image processing software Image J is used to calculate the size metrics of the produced fibers. For this purpose, three FESEM micrographs are produced from random locations on the produced fibers for running the DiameterJ plugin. The diameter distribution of the fibers, before and after heat treatment, is also shown in Figure 5. The micrographs indicate that the fibers are mostly cylindrical, and their diameter predominantly ranges between 100 to 630 nm, with an average diameter of 387.61 nm. The FESEM images do not exhibit any major bead formation. Minimal fiber cross-linking is seen, indicating that the nozzle collector distance is enough for the solvent to evaporate while the fiber jet is travlig towards the collector. The size distribution also indicates that the size distribution and morphology of the fibers remain the same after the heat treatment. The only evident morphological change is the surface smoothness of the heat-treated fibers (Figure 5 (b)) compared to the untreated fibers (Figure 5 (a)). Figure 5 (b) shows that heat treatment of the fibers has made the surface fibers smoother because of changing their morphology to a more crystalline state.

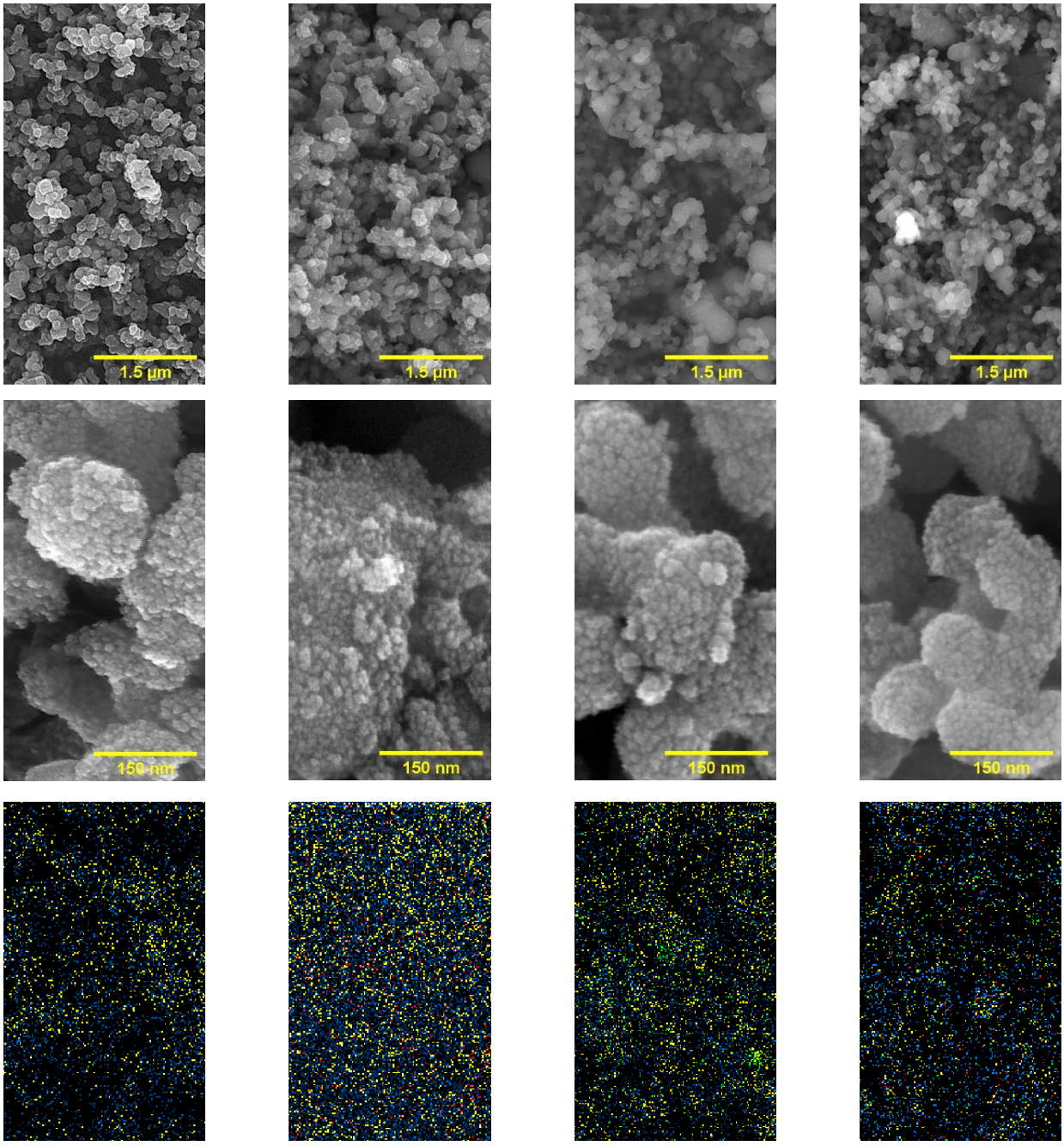

Fig. 3. FESEM and elemental mapping images of a) TiO_2, b) TiO_2/Fe_3O_4, c) TiO_2/Ag and d) Fe_3O_4/TiO_2/Ag. Ti is represented as blue, O, Fe, and Ag are also respectively represented in yellow, red, and green [45].

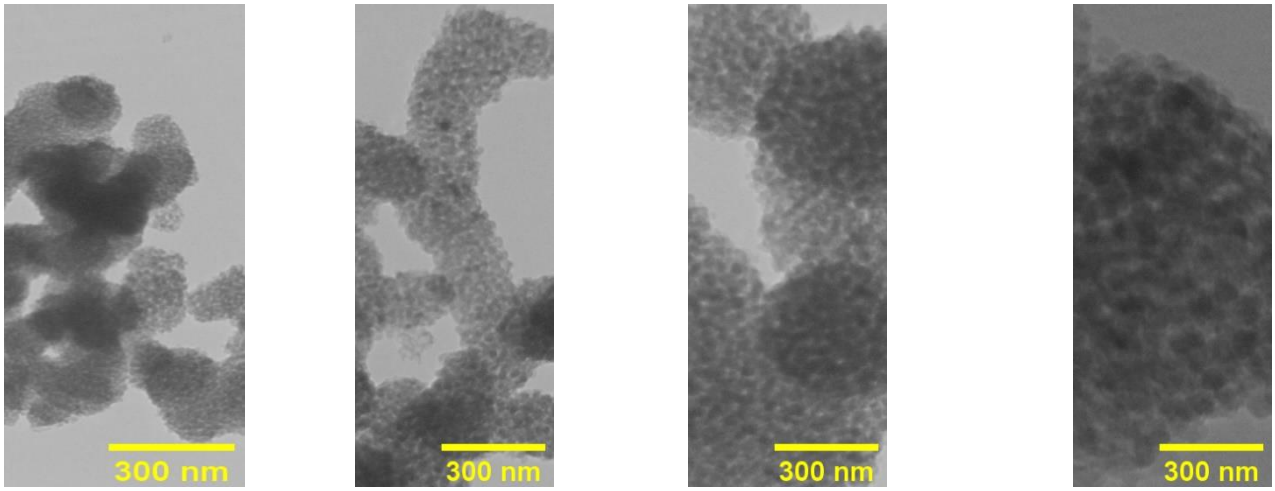

Fig. 4. TEM images of a) TiO_2, b) TiO_2/Fe_3O_4, c) TiO_2/Ag and d) Fe_3O_4/TiO_2/Ag [45].

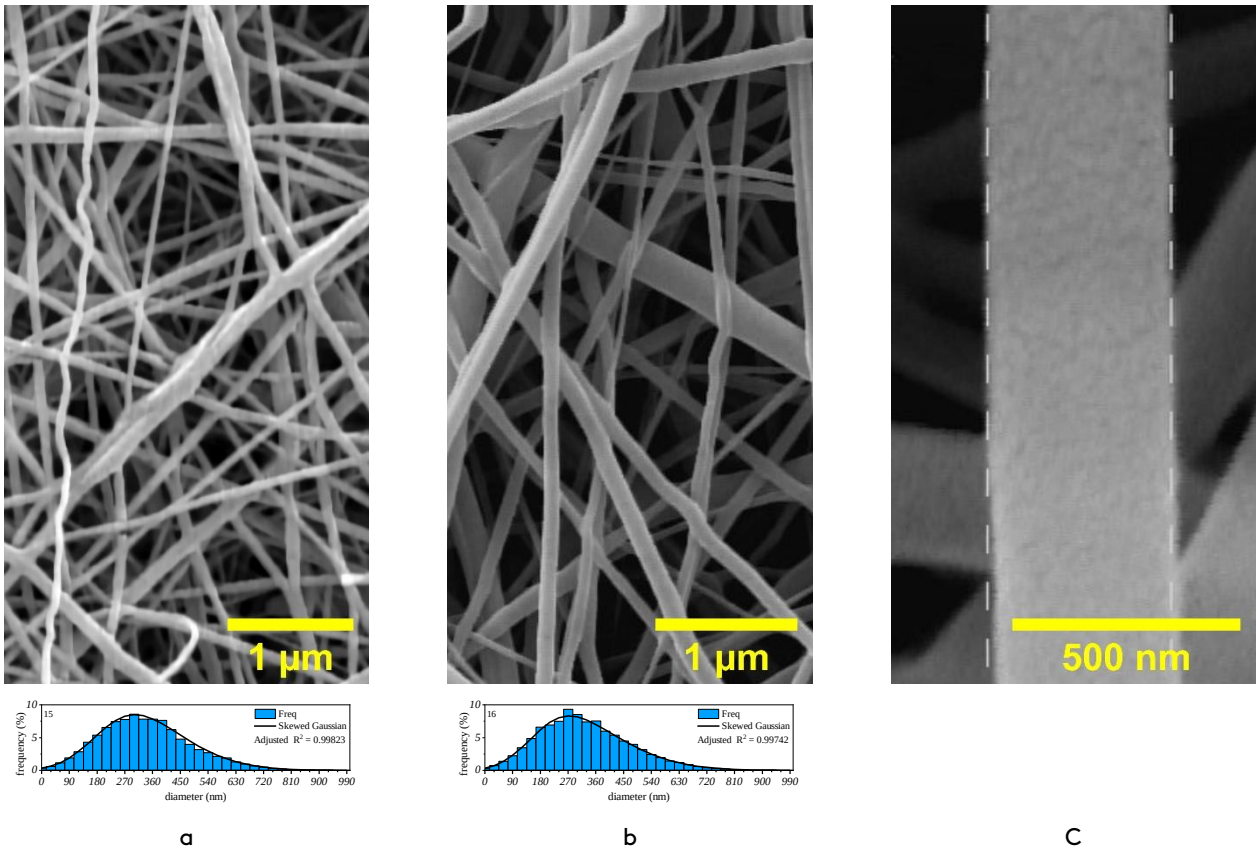

Fig. 5. FESEM images of prepared nanofibers at (a) before heat treatment, (b) after heat treatment (c) close up after heat treatment.

Table 2. Elemental composition of prepared samples [45].

Sample	C (wt%)	N (wt%)	O (wt%)	Ti (wt%)	Fe (wt%)	Ag (wt%)
TiO_2	8.12	14.24	41.68	35.96	0	0
TiO_2/Fe_3O_4	6.31	9.8	40.15	41.99	1.75	0
TiO_2/Ag	10.26	12.43	37.12	36.13	0	4.06
Fe_3O_4/TiO_2/Ag	8.73	12.24	43.84	31.16	1.94	2.09

3.3. Photocatalytic decomposition of 2, 4-dichlorophenol

2,4-dichlorophenol is selected to investigate the catalytic performance of the synthesized samples in an aqueous medium. Table 3 demonstrates the kinetic performance of each catalyst sample in the decomposition process. It is evident that the ternary system of $Fe_3O_4/TiO_2/Ag$ performs better by decomposing approximately 55% of the pollutant in particle form after 180 min of UV/Vis radiation. This result is previously confirmed in the literature [45]. This improvement from single and binary systems is the product of surface plasmon resonance of silver doped nanocomposites, which results in a lower band gap in the ternary system. This means that at lower surface plasmon resonance of Ag, emission of UV/Vis light, results in the departure of a higher energy electron, thus the delivery of electron from Ag to conductive electron band of TiO_2 is accelerated and electron holes are more readily available on Ag surface, which in turn facilitates the oxidation process of pollutant. The migrated O_2 molecules on the surface of TiO_2 keep hold of the electron from the conduction band of the catalyst. As a result, radical species such as $OH^•$ and $O_2^{•-}$ are produced. Finally, the organic pollutant is exposed to these molecules and decomposed. The resulting defect-rich $Fe_3O_4/TiO_2/Ag$ heterojunction produced much more $OH^•$ and $O_2^{•-}$ free radicals on the surfaces of Ag and TiO_2, respectively, which would greatly facilitate the surface redox reactions in photocatalytic processes [51]. Figure 6 shows the mechanism proposed in the present study for the formation of $Fe_3O_4/TiO_2/Ag$ sample and photocatalytic oxidation of 2,4-dichlorophenol over $Fe_3O_4/TiO_2/Ag$ sample. Here we can see that photogenerated electrons and holes are produced on the surface of $Fe_3O_4/TiO_2/Ag$ as UV light strikes it. Fe 2+ and Fe 4+ ions, which are less stable than Fe3+ ions, can be produced by Fe3+ ions by acting as electron and hole traps. Thus it frequently returns to Fe3+ and $OH^•$ and $O_2^{•-}$ radicals are produced as a result [52]. Even though the conduction band of TiO_2 has a higher energy level than the Fermi energy level of Ag, the oscillation hot electron around Ag is stimulated to a higher energy level. Hot electron injection allowed it to do this, and these electrons were also employed to produce free radicals, which increased the photocatalytic activity. In general, photo-excitation, charge separation and migration, and surface oxidation-reduction processes are all components of the photocatalytic reaction [53]. H^+, $OH^•$, and $O_2^{•-}$ are the reactive species produced when photocatalysts are activated. Identifying which reactive species are crucial to the photocatalytic degradation of 2,4-dichlorophenol is vital to comprehend the mechanism by which Fe and Ag degrade 2,4-dichlorophenol. The $OH^•$ radical has been identified as the most significant active species in the photocatalytic oxidation process based on the findings of the intermediate analysis and taking into account the degrading routes proposed by previous literature research [54,55]. The para and ortho locations of the benzene ring are attacked by the $OH^•$ radicals because they are electrophilic and $OH^•$ groups have an electron-donating nature [56].

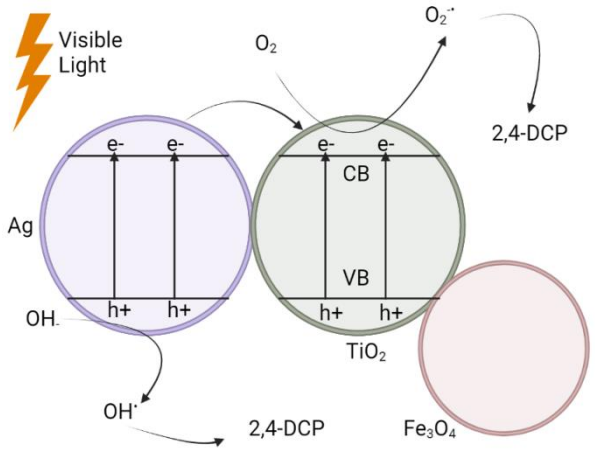

Fig. 6. Photocatalytic oxidation of 2,4-dichlorophenol over $Fe_3O_4/TiO_2/Ag$ photocatalyst under visible irradiation.

The next step was to determine the catalytic performance of nanocatalyst loaded nanofibers. The results in Table 3 indicate that prior to the heat treatment of the nanofiber system, the catalytic activity of the particles drastically decreased to around 38% degradation after 180 min. This is due to the blocking effect of the amorphous and opaque polymer matrix. These optical and morphological properties block the UV/Vis light from reaching particles inside the polymer matrix. On the contrary, after exposing the fiber mats to heat and changing their morphology to a

crystalline form, it can be seen that the catalytic performance of the fiber system is comparable to the catalyst in particle form. To put it in numbers, almost 53% of organic pollutant is decomposed after 180 min of light treatment.

Table 3. Photocatalytic oxidation of 2,4-dichlorophenol by 1 mg/L catalyst under UV/Vis irradiation.

Catalyst	Decomposition % after 180 min
TiO_2	31.35
TiO_2/Fe_3O_4	33.31
TiO_2/Ag	41.37
$Fe_3O_4/TiO_2/Ag$	54.53
$Fe_3O_4/TiO_2/Ag$ loaded nanofibers before heat treatment	38.09
$Fe_3O_4/TiO_2/Ag$ loaded nanofibers after heat treatment	53.12

3.4. Investigation of initial catalyst dosage

To investigate the effect of catalyst loading on degradation rate, different concentrations of catalyst were mixed in the electrospinning solutions. At low photocatalyst loading, the removal of the organic compound 2,4-dichlorophenol increased linearly with the catalyst loading. However, the presence of excess photocatalyst in the electrospinning solutions prevented fiber formation [49]. The reason for this observation was the severe change of electrical conductivities of the electrospinning solution by the introduction of metallic catalyst particles. Fibers were not obtained with a catalyst loading of more than 10 % (w/w). In this regard, the effect of the photocatalyst loading in fibers was investigated for an optimal condition (Figure 7). Thus, the maximum loading capacity of the catalyst on the fibers was chosen as the optimal, which was 10 mg/100 mL for 2, 4-dichlorophenol degradation.

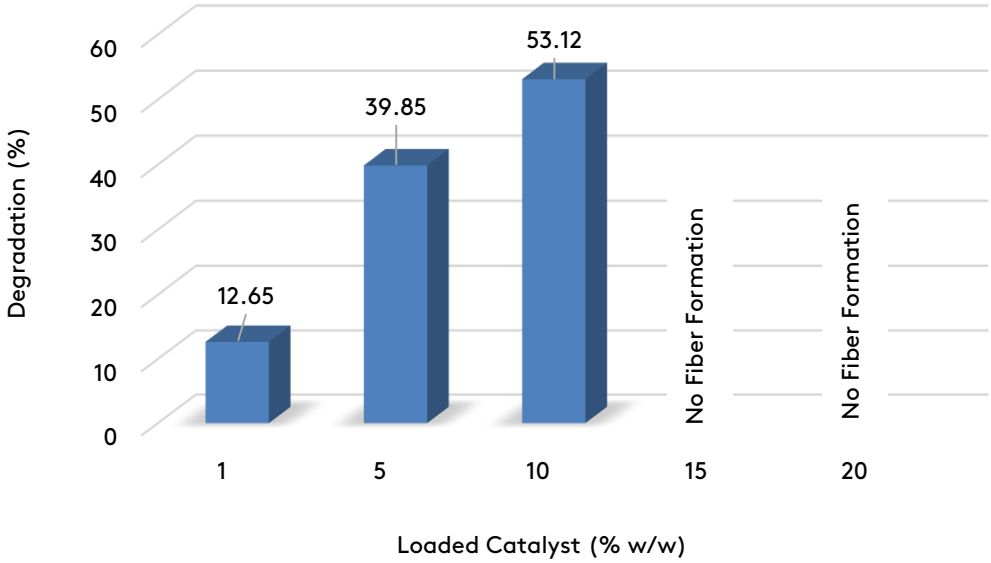

Fig. 7. Effect of photocatalyst loading on degradation of the 2,4-dichlorophnol under visible radiation, 100 mL 2,4-dichlorophnol 40 mg/L, and irradiation time: 180 min.

3.5. Rate study and kinetic performance of prepared catalyst systems

By trying to fit kinetic decomposition data on different functions, it was observed that the reaction takes the form of a first-order system as presented in Eq. (5):

$$\ln(\frac{c}{c_i}) = - Kt \quad (5)$$

where c and c_i are the concentration of pollutant at time t and the initial time, and *K* is the rate constant that is dimensionally compatible with the rest of the parameters. The numerical values of fitness are presented in Table 4. Figure 8 also demonstrates the kinteric degradation performance of the prepared systems. It is evident that the binary systems initiate the degradation process at a higher rate, but as the process continues, the ternary and fiber systems catch up.

The reason for this observation is that the binary systems lack the ability to substitute the active radicals with new ones during the decomposition process. Thus, the process loses pace as it carries on.

Table 4. Kinetic model of 2,4-dichlorophenol decomposition.

Catalyst	K (1/min)	Initial reaction rate (mg/L.min)	R^2
TiO_2	0.0020	0.027	0.9912
TiO_2/Fe_3O_4	0.0022	0.031	0.9813
TiO_2/Ag	0.0029	0.045	0.9918
Fe_3O_4/TiO_2/Ag	0.0043	0.111	0.9856
Fe_3O_4/TiO_2/Ag loaded nanofibers before heat treatment	0.0026	0.021	0.9945
Fe_3O_4/TiO_2/Ag loaded nanofibers after heat treatment	0.0042	0.098	0.9974

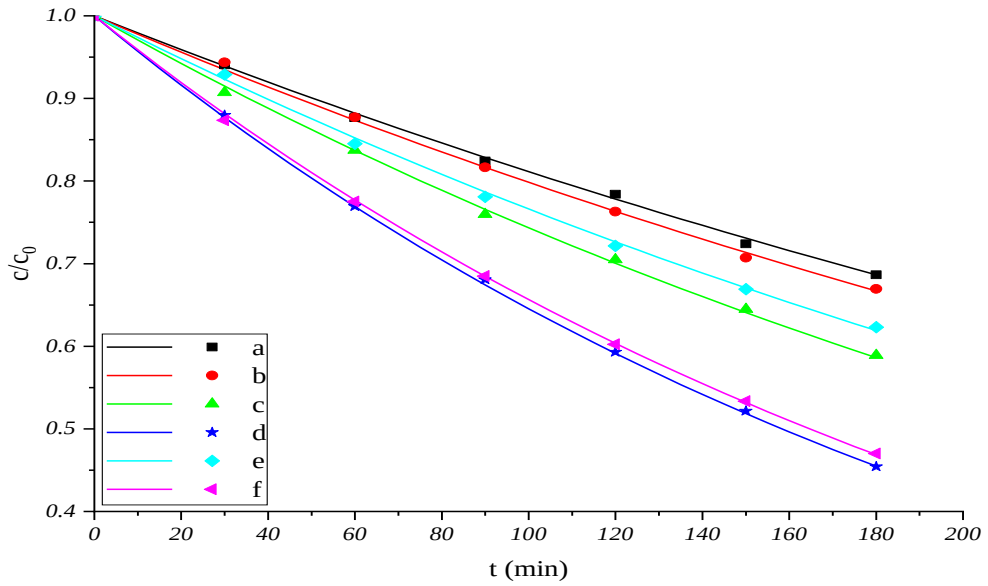

Fig. 8. Decomposition performance of (a) TiO_2 (b) TiO_2/Fe_3O_4 (c) TiO_2/Ag (d) Fe_3O_4/TiO_2/Ag and Fe_3O_4/TiO_2/Ag loaded nanofibers before (e) heat treatment and (f) after treatment. Lines represent first order model and dots represent real data.

3.6. Reusability of produced nanocatalysts

The main objective of this paper was to prepare a reusable and recyclable photocatalyst system for the treatment of organic water pollutants. Previously, it was shown that Fe_3O_4 based nanocomposites could successfully be recycled using an external magnetic force [32]. Those studies utilized a magnet to extract the magnetic particles for reuse. The downside of this approach was its slow application and of delicate handling requirementls, which contradicted industrial process requirements. Thus, this study solved this problem by fixing the nanocatalysts on a nanofibrous system that provided a large specific surface area and simple and fast extraction of the catalyst system from the process medium. Fig. 9 compares the reusability of the ternary system as a solitary system loaded on a fibrous polymer matrix. It is evident that in addition to the separation and recycling being faster and easier to implement in the case of catalyst-loaded nanofibers, it also yields better results in the second and third runs. This occurs because, in this method, larger amounts of catalyst particles are preserved at the extraction stage compared to magnetic separation. Thus, the second and third runs perform reasonably better compared to the particle system.

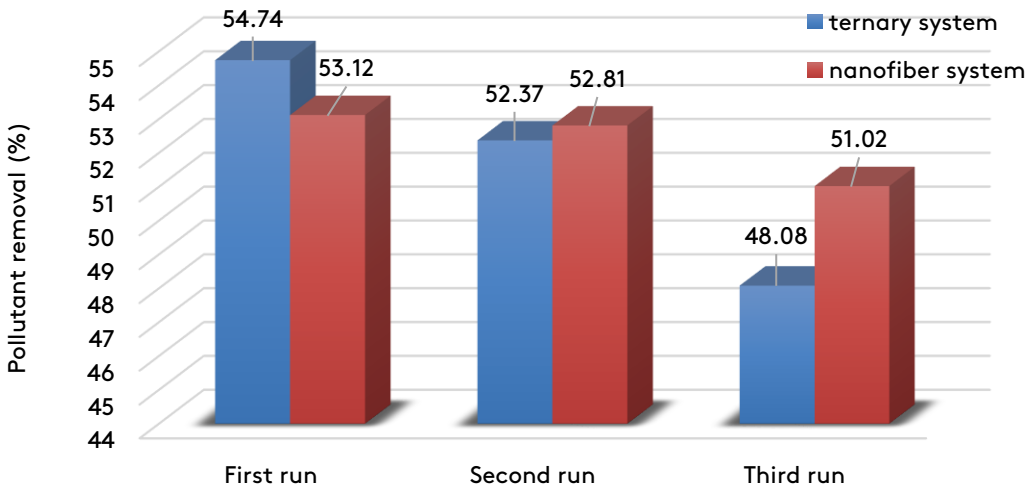

Fig. 9. Reusability comparison of $Fe_3O_4/TiO_2/Ag$ photocatalytic system as a particle [45] and as active agent loaded on electrospun nanofibers after 3 passes of UV/Vis treatment each for 3 h. All cases started with a concentration of 40 mg/L pollutant.

4. Conclusions

This paper studied the possibility of loading $Fe_3O_4/TiO_2/Ag$ photocatalytic particles on PCL/PEG electrospun nanofiber. FESEM, TEM, XRD, UV/Vis spectrophotometry, and elemental mapping techniques were implemented to investigate the effect of catalyst loaded nanofiber on the oxidative decomposition of 2, 4-dichlorophenol. It was observed that by physically attaching the particles to the polymer nanofibers, a desirable photocatalytic activity was observed. The newly presented system introduced an improvement regarding reusability by eliminating the need to separate catalyst particles from the oxidationmedium.

References

[1] Ahmed, S., Rasul, M. G., Brown, R., Hashib, M. A. (2011). Influence of parameters on the heterogeneous photocatalytic degradation of pesticides and phenolic contaminants in wastewater: a short review. *Journal of environmental management*, 92(3), 311-330.

[2] Babuponnusami, A., Muthukumar, K. (2014). A review on Fenton and improvements to the Fenton process for wastewater treatment. *Journal of environmental chemical engineering*, *2*(1), 557-572.

[3] Devi, L. G., Kavitha, R. (2013). A review on nonmetal ion doped titania for the photocatalytic degradation of organic pollutants under UV/solar light: Role of photogenerated charge carrier dynamics in enhancing the activity. *Applied catalysis B: Environmental*, *140*, 559-587.

[4] Cabiscol Català, E., Tamarit Sumalla, J., Ros Salvador, J. (2000). Oxidative stress in bacteria and protein damage by reactive oxygen species. *International microbiology, 2000, 3 (1)*, 3-8.

[5] Valavanidis, A., Vlahogianni, T., Dassenakis, M., Scoullos, M. (2006). Molecular biomarkers of oxidative stress in aquatic organisms in relation to toxic environmental pollutants. *Ecotoxicology and environmental safety*, *64*(2), 178-189.

[6] Aguilar, C. H., Pandiyan, T., Arenas-Alatorre, J. A., Singh, N. (2015). Oxidation of phenols by TiO_2Fe_3O4M (M= Ag or Au) hybrid composites under visible light. *Separation and purification technology*, *149*, 265-278.

[7] J. Bergendahl and J. O'Shaughnessy, "Applications of advanced oxidation for wastewater treatment," in *international business and education conference "A focus on water management", Worcester polytechnic Institute*, 2004.

[8] Daghrir, R., Drogui, P., Robert, D. (2013). Modified TiO_2 for environmental photocatalytic applications: a review. *Industrial and*

engineering chemistry research, *52*(10), 3581-3599.

[9] Kumar, S. G., Devi, L. G. (2011). Review on modified TiO_2 photocatalysis under UV/visible light: selected results and related mechanisms on interfacial charge carrier transfer dynamics. *The journal of physical chemistry A*, *115*(46), 13211-13241.

[10] Sarteep, Z., Ebrahimian Pirbazari, A., Aroon, M. A. (2016). Silver doped TiO2 nanoparticles: preparation, characterization and efficient degradation of 2, 4-dichlorophenol under visible light. *Journal of water and environmental Nanotechnology*, *1*(2), 135-144.

[11] Blake, D. M., Webb, J., Turchi, C., Magrini, K. (1991). Kinetic and mechanistic overview of TiO2-photocatalyzed oxidation reactions in aqueous solution. *Solar energy materials*, *24*(1-4), 584-593.

[12] Choi, H., Al-Abed, S. R., Dionysiou, D. D., Stathatos, E., Lianos, P. (2010). TiO2-based advanced oxidation nanotechnologies for water purification and reuse. *Sustainability science and engineering*, *2*, 229-254.

[13] Guo, M., Du, J. (2012). First-principles study of electronic structures and optical properties of Cu, Ag, and Au-doped anatase TiO_2. *Physica B: Condensed matter*, *407*(6), 1003-1007.

[14] Kiyonaga, T., Mitsui, T., Torikoshi, M., Takekawa, M., Soejima, T., Tada, H. (2006). Ultrafast photosynthetic reduction of elemental sulfur by Au nanoparticle-loaded TiO2. *The journal of physical chemistry B*, *110*(22), 10771-10778.

[15] Jiang, L., Wang, Y., Feng, C. (2012). Application of photocatalytic technology in environmental safety. *Procedia engineering*, *45*, 993-997.

[16] Fang, Y., Jiao, Y., Xiong, K., Ogier, R., Yang, Z. J., Gao, S., Kall, M. (2015). Plasmon enhanced internal photoemission in antenna-spacer-mirror based Au/TiO_2 nanostructures. *Nano letters*, *15*(6), 4059-4065.

[17] Lin, Y., Geng, Z., Cai, H., Ma, L., Chen, J., Zeng, J., Wang, X. (2012). Ternary graphene–TiO_2–Fe_3O_4 nanocomposite as a recollectable photocatalyst with enhanced durability. *European journal of inorganic chemistry*, *2012*(28), 4439-4444.

[18] Dominguez, S., Ribao, P., Rivero, M. J., Ortiz, I. (2015). Influence of radiation and TiO2 concentration on the hydroxyl radicals generation in a photocatalytic LED reactor. Application to dodecylbenzenesulfonate degradation. *Applied catalysis B: Environmental*, *178*, 165-169.

[19] Morales, J., Maldonado, A., Olvera, M. D. L. L. (2013, September). Synthesis and characterization of nanoestructured TiO_2 anatase-phase powders obtained by the homogeneous precipitation method. In*2013 10th international conference on electrical engineering, computing science and automatic control (CCE)* (pp. 391-394). IEEE.

[20] Ahlborg, U. G., Thunberg, T. M., Spencer, H. C. (1980). Chlorinated phenols: occurrence, toxicity, metabolism, and environmental impact. *CRC critical reviews in toxicology*, *7*(1), 1-35.

[21] Mohy Eldin, M. S., Aggour, Y. A., El-Aassar, M. R., Beghet, G. E., Atta, R. R. (2016). Development of nano-crosslinked polyacrylonitrile ions exchanger particles for dyes removal. *Desalination and water treatment*, *57*(9), 4255-4266.

[22] Elzain, A. A., El-Aassar, M. R., Hashem, F. S., Mohamed, F. M., Ali, A. S. (2019). Removal of methylene dye using composites of poly (styrene-co-acrylonitrile) nanofibers impregnated with adsorbent materials. *Journal of molecular liquids*, *291*, 111335.

[23] Lee, H. C., In, J. H., Kim, J. H., Hwang, K. Y., Lee, C. H. (2005). Kinetic analysis for decomposition of 2, 4-dichlorophenol by supercritical water oxidation. *Korean journal of chemical engineering*, *22*(6), 882-888.

[24] Alsohaimi, I. H., El-Aassar, M. R., Elzain, A. A., Alshammari, M. S., Ali, A. S. (2020). Development of activated carbon-impregnated alginate* β-cyclodextrin/gelatin beads for highly performance sorption of 2, 4-dichlorophenol from wastewater. *Journal of materials research and technology*, *9*(3), 5144-5153.

[25] El-Aassar, M. R., Alsohaimi, I. H., Ali, A. S., Elzain, A. A. (2020). Removal of phenol and Bisphenol A by immobilized Laccase on poly (Acrylonitrile-co-Styrene/Pyrrole) nanofibers.

Separation science and technology, *55*(15), 2670-2678.

[26] Dionysiou, D. D., Khodadoust, A. P., Kern, A. M., Suidan, M. T., Baudin, I., Laîné, J. M. (2000). Continuous-mode photocatalytic degradation of chlorinated phenols and pesticides in water using a bench-scale TiO2 rotating disk reactor. *Applied catalysis B: environmental*, *24*(3-4), 139-155.

[27] Arnoldsson, K., Andersson, P. L., Haglund, P. (2012). Formation of environmentally relevant brominated dioxins from 2, 4, 6,-tribromophenol via bromoperoxidase-catalyzed dimerization. *Environmental science and technology*, *46*(13), 7239-7244.

[28] Bandara, J., Mielczarski, J. A., Lopez, A., Kiwi, J. (2001). 2. Sensitized degradation of chlorophenols on iron oxides induced by visible light: comparison with titanium oxide. *Applied catalysis B: Environmental*, *34*(4), 321-333.

[29] Yan, H., Wang, R., Liu, R., Xu, T., Sun, J., Liu, L., Wang, J. (2021). Recyclable and reusable direct Z-scheme heterojunction CeO_2/TiO_2 nanotube arrays for photocatalytic water disinfection. *Applied catalysis B: Environmental*, *291*, 120096.

[30] Donga, C., Mishra, S. B., Abd-El-Aziz, A. S., Mishra, A. K. (2021). Advances in graphene-based magnetic and graphene-based/TiO2 nanoparticles in the removal of heavy metals and organic pollutants from industrial wastewater. *Journal of inorganic and organometallic polymers and materials*, *31*(2), 463-480.

[31] Al-Madanat, O., Curti, M., Günnemann, C., AlSalka, Y., Dillert, R., Bahnemann, D. W. (2021). TiO2 photocatalysis: Impact of the platinum loading method on reductive and oxidative half-reactions. *Catalysis today*, *380*, 3-15.

[32] Zhang, L., Wu, Z., Chen, L., Zhang, L., Li, X., Xu, H., Zhu, G. (2016). Preparation of magnetic Fe_3O_4/TiO_2/Ag composite microspheres with enhanced photocatalytic activity. *Solid state sciences*, *52*, 42-48.

[33] Fàbrega, C., Andreu, T., Cabot, A., Morante, J. R. (2010). Location and catalytic role of iron species in TiO2: Fe photocatalysts: An EPR study. *Journal of photochemistry and photobiology A: Chemistry*, *211*(2-3), 170-175.

[34] Zhao, Y., Tao, C., Xiao, G., Wei, G., Li, L., Liu, C., Su, H. (2016). Controlled synthesis and photocatalysis of sea urchin-like Fe_3O_4@ TiO_2@ Ag nanocomposites. *Nanoscale*, *8*(9), 5313-5326.

[35] Zhu, J., Ren, J., Huo, Y., Bian, Z., Li, H. (2007). Nanocrystalline Fe/TiO2 visible photocatalyst with a mesoporous structure prepared via a nonhydrolytic sol– gel route. *The journal of physical chemistry C*, *111*(51), 18965-18969.

[36] Mahmiani, Y., Sevim, A. M., Gül, A. (2016). Photocatalytic degradation of 4-chlorophenol under visible light by using TiO2 catalysts impregnated with Co (II) and Zn (II) phthalocyanine derivatives. *Journal of photochemistry and photobiology A: Chemistry*, *321*, 24-32.

[37] Yang, M. Q., Zhang, N., Wang, Y., Xu, Y. J. (2017). Metal-free, robust, and regenerable 3D graphene–organics aerogel with high and stable photosensitization efficiency. *Journal of catalysis*, *346*, 21-29.

[38] Karakas, K., Celebioglu, A., Celebi, M., Uyar, T., Zahmakiran, M. (2017). Nickel nanoparticles decorated on electrospun polycaprolactone/chitosan nanofibers as flexible, highly active and reusable nanocatalyst in the reduction of nitrophenols under mild conditions. *Applied catalysis B: Environmental*, *203*, 549-562.

[39] Wang, C., Yin, J., Han, S., Jiao, T., Bai, Z., Zhou, JPeng, Q. (2019). Preparation of palladium nanoparticles decorated polyethyleneimine/polycaprolactone composite fibers constructed by electrospinning with highly efficient and recyclable catalytic performances. *Catalysts*, *9*(6), 559.

[40] Kim, G. H. (2008). Electrospun PCL nanofibers with anisotropic mechanical properties as a biomedical scaffold. *Biomedical materials*, *3*(2), 025010.

[41] Koo, K. N., Ismail, A. F., Othman, M. H. D., Bidin, N., & Rahman, M. A. (2019). Preparation and characterization of superparamagnetic magnetite (Fe3O4) nanoparticles: A short

review. *Malaysian J. Fundam. Appl. Sci*, *15*(1), 23-31.

[42] Hui, B. H., Salimi, M. N. (2020, February). Production of iron oxide nanoparticles by co-precipitation method with optimization studies of processing temperature, pH and stirring rate. In *IOP conference series: Materials science and engineering* (Vol. 743, No. 1, p. 012036). IOP Publishing.

[43] Wang, R., Wang, X., Xi, X., Hu, R., Jiang, G. (2012). Preparation and photocatalytic activity of magnetic $Fe_3O_4/SiO_2/TiO_2$ composites. *Advances in materials science and engineering*, *2012*.

[44] Shi, L., He, Y., Wang, X., Hu, Y. (2018). Recyclable photo-thermal conversion and purification systems via Fe_3O_4@ TiO_2 nanoparticles. *Energy conversion and management*, *171*, 272-278.

[45] Esmaeili, N., Pirbazari, A. E., Khodaee, Z. (2018). Visible-light active and magnetically recyclable Ag-coated Fe_3O_4/TiO_2 nanocomposites for efficient photocatalytic oxidation of 2, 4-dichlorophenol. *Desalination and Water Treatment*, *114*, 251-264.

[46] Zavan, B., Gardin, C., Guarino, V., Rocca, T., Cruz Maya, I., Zanotti, F., Gasbarro, V. (2021). Electrospun PCL-based vascular grafts: In vitro tests. *Nanomaterials*, *11*(3), 751.

[47] Reis, I. A., Cunha Claro, P. I., Marcomini, A. L., Capparelli Mattoso, L. H., da Silva, S. P., de Sena Neto, A. R. (2021). Annealing and crystallization kinetics of poly (lactic acid) pieces obtained by additive manufacturing. *Polymer engineering and science*, *61*(7), 2097-2104.

[48] Rahmayeni, R., Arief, S., Stiadi, Y., Rizal, R., Zulhadjri, Z. (2012). Synthesis of magnetic nanoparticles of TiO_2-$NiFe_2O_4$: characterization and photocatalytic activity on degradation of rhodamine B. *Indonesian journal of chemistry*, *12*(3), 229-234.

[49] Morales, J., Maldonado, A., Olvera, M. D. L. L. (2013, September). Synthesis and characterization of nanoestructured TiO_2 anatase-phase powders obtained by the homogeneous precipitation method. In *2013 10th International conference on electrical engineering, computing science and automatic control (CCE)* (pp. 391-394). IEEE.

[50] Roy, K., Sarkar, C. K., Ghosh, C. K. (2015). Photocatalytic activity of biogenic silver nanoparticles synthesized using potato (Solanum tuberosum) infusion. *Spectrochimica Acta Part A: Molecular and biomolecular spectroscopy*, *146*, 286-291.

[51] Ning, P., Chen, H., Pan, J., Liang, J., Qin, L., Chen, D., Huang, Y. (2020). Surface defect-rich gC_3N_4/TiO_2 Z-scheme heterojunctions for efficient photocatalytic antibiotic removal: rational regulation of free radicals and photocatalytic mechanism. *Catalysis science and technology*, *10*(24), 8295-8304.

[52] Yeo, S. J., Kang, H., Kim, Y. H., Han, S., Yoo, P. J. (2012). Layer-by-layer assembly of polyelectrolyte multilayers in three-dimensional inverse opal structured templates. *ACS applied materials and interfaces*, *4*(4), 2107-2115.

[53] Li, H., Yin, S., Wang, Y., Sato, T. (2013). Efficient persistent photocatalytic decomposition of nitrogen monoxide over a fluorescence-assisted $CaAl_2O_4$:(Eu, Nd)/ (Ta, N)-codoped $TiO2/Fe_2O_3$. *Applied catalysis B: Environmental*, *132*, 487-492.

[54] Li, X., Cubbage, J. W., Tetzlaff, T. A., Jenks, W. S. (1999). Photocatalytic degradation of 4-chlorophenol. 1. The hydroquinone pathway. *The journal of organic chemistry*, *64*(23), 8509-8524.

[55] Li, S., Xu, Y., Wang, X., Guo, Y., Mu, Q. (2016). Catalytic degradation of 4-chlorophenol with La/TiO_2 in a dielectric barrier discharge system. *RSC advances*, *6*(34), 28994-29002.

[56] Asiltürk, M., Sayılkan, F., Arpaç, E. (2009). Effect of Fe3+ ion doping to TiO2 on the photocatalytic degradation of Malachite green dye under UV and vis-irradiation. *Journal of photochemistry and photobiology A: Chemistry*, *203*(1), 64-71.

[57] Wu, L., Li, A., Gao, G., Fei, Z., Xu, S., Zhang, Q. (2007). Efficient photodegradation of 2, 4-dichlorophenol in aqueous solution catalyzed by polydivinylbenzene-supported zinc phthalocyanine. *Journal of molecular catalysis A: Chemical*, *269*(1-2), 183-189.